HHS Public Access

Author manuscript

J Comp Neurol. Author manuscript; available in PMC 2020 April 01.

Published in final edited form as:

J Comp Neurol. 2019 April 01; 527(5): 942–956. doi:10.1002/cne.24557.

MIDLINE THALAMIC INPUTS TO THE AMYGDALA: ULTRASTRUCTURE AND SYNAPTIC TARGETS

Alon Amir[1], **Jean-Francois Paré**[2], **Yoland Smith**[2], and **Denis Paré**[1]

[(1)]Center for Molecular and Behavioral Neuroscience, Rutgers University-Newark, NJ

[(2)]Yerkes National Primate Research Center and Department of Neurology, Emory University, 954 Gatewood Road, Atlanta, GA 30329.

Abstract

One of the main subcortical inputs to the basolateral nucleus of the amygdala (BL) originates from a group of dorsal thalamic nuclei located at or near the midline, mainly from the central medial (CMT) and paraventricular (PVT) nuclei. Although similarities between the responsiveness of BL, CMT, and PVT neurons to emotionally arousing stimuli suggest that these thalamic inputs exert a significant influence over BL activity, little is known about the synaptic relationships that mediate these effects. Thus, the present study used *Phaseolus vulgaris*-leucoagglutinin (PHAL) anterograde tracing and electron microscopy to shed light on the ultrastructural properties and synaptic targets of CMT and PVT axon terminals in the rat BL. Virtually all PHAL-positive CMT and PVT axon terminals formed asymmetric synapses. While CMT and PVT axon terminals generally contacted dendritic spines, a substantial number ended on dendritic shafts. To determine if these dendritic shafts belonged to principal or local-circuit cells, we used immunoreactivity for calcium/calmodulin-dependent protein kinase II (CAMKIIα) as a selective marker of principal BL neurons. In most cases, dendritic shafts postsynaptic to PHAL-labeled CMT and PVT terminals were immunopositive for CaMKIIα. Overall, these results suggest that CMT and PVT inputs mostly target principal BL neurons such that when CMT or PVT neurons fire, little feed-forward inhibition counters their excitatory influence over principal cells. These results are consistent with the possibility that CMT and PVT inputs constitute major determinants of BL activity.

Graphical Abstract

Correspondence should be sent to: Denis Paré, Center for Molecular and Behavioral Neuroscience, Rutgers State University, 197 University Ave., Newark, NJ 07102, USA, Tel: 973-353-3251, Fax: 973-353-1255, pare@andromeda.rutgers.edu.

ROLE OF AUTHORS: All authors had full access to all the data in the study and take responsibility for the integrity of the data and the accuracy of the data analysis. Study concept and design: DP, YS. Acquisition of data: AA, JFP. Analysis and interpretation of data: AA, DP, YS, JFP. Drafting of the manuscript: DP, YS. Critical revision of the manuscript for important intellectual content: AA, DP, YS, JFP. Statistical analysis: DP. Obtained funding: DP, YS. Administrative and technical support: JFP. Study supervision: DP, YS.

CONFLICT OF INTEREST STATEMENT: The authors state that they have no conflict of interest.

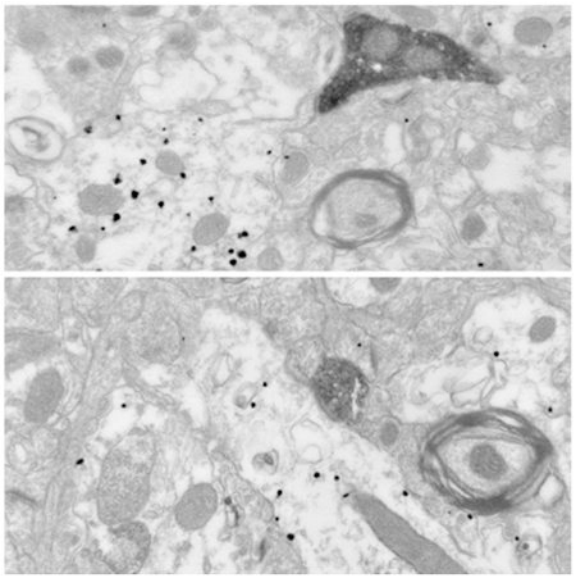

We combined tracing and electron microscopy to identify the targets of midline thalamic (MTh) axon terminals in the basolateral amygdala (BL). MTh axon terminals formed asymmetric synapses with neurons that were immunoreactive for CAMKIIα, a marker of principal neurons. Thus, MTh inputs exert a prevalently excitatory influence over principal cells.

Keywords

Electron microscopy; tract-tracing; thalamus; amygdala; CAMKIIα; RRID RGD_734476; RRID AB_2336656; RRID AB_2313686; RRID AB_447192; RRID AB_2313606; RRID AB_2637031

INTRODUCTION

Several dorsal thalamic nuclei at or near the midline densely innervate the amygdala, particularly its basolateral (BL) and central (CeA) nuclei (Russchen, 1982; Turner & Herkenham, 1991; Vertes, Hoover, Do Valle, Sherman, & Rodriguez, 2006; Vertes & Hoover, 2008; Vertes, Hoover, & Rodriguez, 2012). The thalamic nuclei at the origin of these projections include the rhomboid, parataenial, reuniens, paraventricular (PVT), and central medial (CMT) thalamic nuclei, the latter two respectively sending the densest projections to Ce and BL, but contributing much weaker projections to other amygdala nuclei (Vertes, Hoover, Do Valle, Sherman, & Rodriguez, 2006; Vertes & Hoover, 2008; Vertes, Hoover, & Rodriguez, 2012). Contrasting with the reciprocity of cortico-thalamic projections (reviewed in Jones, 2007), BL does not project back to PVT and CMT, but to the mediodorsal thalamic nucleus (Krettek & Price, 1977).

At present, the role of these thalamic afferents to the amygdala is unclear. Indeed, midline thalamic nuclei have been implicated in a staggering array of functions and disorders (reviewed in Benarroch, 2008; Price & Drevets, 2010; Van der Werf, Witter, & Groenewegen, 2002). With respect to PVT, a recurrent theme in the literature is the exceptional sensitivity of neurons in this nucleus to a variety of psychogenic and physical

stressors, typically assessed using Fos expression (Bubser & Deutch, 1999; Lkhagvasuren et al., 2014; Otake, Kin, & Nakamura, 2002; Spencer, Fox, & Day, 2004; Timofeeva & Richard, 2001). However, PVT is not only recruited by aversive, but also by positively valenced stimuli, including natural rewards, drugs of abuse, and the cues associated with them (Brown, Robertson, & Fibiger, 1992; Deutch, Bubser, & Young, 1998; Franklin & Druhan, 2000; Igelstrom, Herbison, & Hyland, 2010; Johnson, Revis, Burdick, & Rhodes, 2010). Together, these studies suggest that PVT neurons are responsive to emotionally charged stimuli, irrespective of valence.

In contrast, CMT appears to be mainly involved in the processing of aversive signals. Indeed, nociceptive (but not innocuous) stimuli induce Fos expression in CMT neurons (Kuroda, Yorimae, Yamada, Furuta, & Kim, 1995). Moreover, intra-CMT injections of lidocaine attenuate formalin-induced pain behaviors (McKenna & Melzak, 1994). However, the CMT also plays a critical role in the maintenance of awareness. Indeed, intra-CMT injections of minute amounts of nicotine elicit arousal from deep anesthesia (Alkire, McReynolds, Hahn, & Trivedi, 2007; Leung, Luo, Ma, & Herrick, 2014). Moreover, it was reported that alterations in CMT activity precipitate the loss of consciousness that occurs at the onset of slow-wave sleep and the induction of general anesthesia (Baker et al., 2014).

Although the PVT and CMT might influence some of these behaviors via the amygdala, these projections have received little attention so far. Instead, investigators have focused on inputs from the posterior thalamic complex because of their involvement in classical fear conditioning. Yet, recent findings suggest that even the expression of conditioned fear responses is dependent on inputs from midline thalamic nuclei (Do-Monte, Quiñones-Laracuente, & Quirk, 2015; Padilla-Coreano, Do-Monte, & Quirk, 2012). Thus, the present study was undertaken to characterize the ultrastructural features and synaptic targets of PVT and CMT axon terminals in the basolateral (BL) and central (CeA) nuclei of the amygdala. To this end, we used anterograde tracing with *Phaseolus vulgaris*-leucoagglutinin (PHAL) to label thalamic terminals. In the BL, PHAL immunostaining was combined with immunocytochemistry for calcium/calmodulin-dependent protein kinase II (CAMKIIα), a marker of principal cells, at the light and electron microscopic (EM) level.

MATERIALS AND METHODS

Animals and Tract-tracing

Surgical procedures were conducted in accordance with the NIH Guide for the Care and Use of Laboratory Animals and approved by the Institutional Animal Care and Use Committees of Rutgers University. We used male Sprague-Dawley rats (n=18) weighing 220-320 g (RRID RGD_734476, Charles River Laboratories, Wilmington, MA). Rats were maintained on a 12-hour light/dark cycle with *ad libitum* food and water. After habituation to the animal facility and handling, rats were anesthetized with isoflurane (~2%, inhaled) and administered atropine (0.05 mg/kg, i.m.) to aid breathing. After shaving their scalp and placing the rats in a stereotaxic apparatus, we injected the local analgesic bupivacaine (0.125% solution, s.c.) at the site to be incised. Then, using sterile procedures, the scalp was incised above the thalamic region of interest, small holes were drilled into the skull, the *dura mater* was opened, and rats received unilateral injections of the anterograde tracer PHAL

(Catalog # L-1110, RRID AB_2336656, Vector Laboratories, Burlingame, CA) in CMT or PVT.

The stereotaxic coordinates we used were (in mm relative to bregma for the antero-posterior –AP– and medio-lateral –ML– dimensions, and from the *dura mater* for the dorso-ventral –DV– dimension): CMT (AP, −2.4; ML, 0; DV, 6.2); PVT (AP, −3.2; ML, 0; DV, 4.9). These coordinates were determined using Paxinos & Watson's (2007) stereotaxic atlas of the rat brain. Because CMT and PVT are located along the midline, the pipette was inserted using an oblique (18 degrees), lateromedial approach. PHAL (4%) was dissolved in 0.01M phosphate buffer (PB; pH 8.0) and injected iontophoretically through a glass pipette (tip diameter: 25-30 μm) using positive 7 μA current pulses (2 sec on / 2 sec off) for 40 min.

Ten to twelve days after the PHAL injection, under deep isoflurane anesthesia, rats were perfused through the heart with 150 ml of a cold oxygenated Ringer solution, followed by 500 ml of a fixative solution containing 4% depolymerized paraformaldehyde and 0.1% glutaraldehyde in 0.1M PB (pH 7.4). Their brains were then removed, cut into blocks containing the thalamus and amygdala, post-fixed in the same fixative for 24 hours, and sectioned at 60 μm using a vibrating microtome. Brain sections were collected in PBS (0.01 M; pH 7.4) until further processing.

Immunohistochemistry

Overview of methods and specificity of antibodies.—For light and electron microscopy (EM), we detected PHAL with the immunoperoxidase method, using diaminobenzidine (DAB) as a chromogen. CAMKIIα immunoreactivity was detected using the pre-embedding immunogold-silver intensification procedure. We used a rabbit anti-PHAL (1:1000, catalog # AS-2300, lot # Y0806, RRID AB_2313686, Vector Labs, Burlingame, CA) antibody. Of note, no differentiated labeling was seen when the PHAL antibody was used on brain sections obtained from animals that did not receive PHAL injections. To detect CAMKIIα immunoreactivity, we used a mouse monoclonal (6G9) anti-CaMKIIα antibody (Abcam, Cambridge, MA; catalog # AB22609, lot # GR30131-1, RRID AB_447192) that was prepared against purified CaMKIIα. The company Abcam evaluated this antibody for activity and specificity. Western blot analysis yielded positive signals in human, rat and mouse whole brain tissue lysates, detected as a band with a molecular weight of 50kDa. Of note, this antibody detects CaMKIIα in its phosphorylated and non-phosphorylated forms (Erondu & Kennedy, 1985; Jung, Kim, & Hoffman, 2008). Expected reactivity also includes the delta and gamma isoforms, but not the beta isoform.

Immunohistochemistry for light microscopic observations.—PHAL was revealed by incubating brain sections in sodium borohydride (1% in PBS) for 20 min at room temperature, repeatedly rinsing them in PBS (0.01M, pH 7.4), and incubating them for 60 min in a blocking solution containing 1% bovine serum albumin (BSA), 1% normal goat serum (NGS), and 0.03% Triton X-100 in PBS. Sections were then incubated in rabbit anti-PHAL antibody (1:1000, Vector Labs, Burlingame, CA) overnight. On the following day, sections were rinsed in PBS (3 × 10 min), incubated for 90 min in biotinylated goat anti-rabbit IgG (1:200, catalog # BA-1000, lots# ZA0520 and ZB1007, RRID AB_2313606,

Vector Laboratories, Burlingame, CA), and then rinsed in PBS (3 × 10 min). Last, sections were incubated in the avidin-biotin peroxidase complex (ABC, Vector Labs, Burlingame, CA) for 90 min before being rinsed in TRIS buffer (0.05M, pH 7.6). Peroxidase was revealed using a solution of 0.025% diaminobenzidine (DAB) and 0.006% hydrogen peroxide in TRIS buffer (TBS; 0.05M, pH 7.6). Sections were then rinsed in 0.01 M PBS (pH 7.4). At the end of the incubations, they were mounted onto glass slides, air-dried, dehydrated in a graded series of alcohol, and coverslipped in Cytoseal XYL mounting medium (ThermoFisher Scientific, Waltham, MA) for light microscopic observations.

Immunohistochemical procedures for EM observations.—Sections were first incubated in sodium borohydride (1% in PBS) for 20 min at room temperature, repeatedly rinsed in PBS (0.01M, pH 7.4), and then placed in a cryoprotectant solution (25% sucrose and 10% glycerol in PB, 0.05 M, pH 7.4) for 20 min. They were then placed in a −80°C freezer for an additional 20 min. This procedure permeabilizes cell membranes and facilitates penetration of antibodies in the tissue. Sections were then thawed, washed in PBS, and processed as above with two exceptions: Triton X-100 was not used and the incubation in the primary antibody solution lasted 48 hours at 4°C. Next, sections were rinsed in PB, post-fixed for 20 min in osmium tetroxide (1% in PB), and rinsed many times in PB. Next, sections were dehydrated in graded series of alcohol and propylene oxide. Uranyl acetate (1%) was added to the 70% alcohol for 35 minutes to improve contrast in the EM. Sections were then embedded in Durcupan resin (Fluka, Gymea, Australia), transferred to glass slides, coverslipped, and left in an oven at 60°C for two days. After polymerization of the resin, the regions of interest were cut, removed from the glass slides, adhered onto resin blocks, and trimmed in a trapezoidal shape before being resectioned with an ultramicrotome (Ultracut-T, Leica Microsystems, Wetzlar, Germany) at a thickness of 60-70 nm with a 45°-diamond knife. Ultrathin sections were then collected onto copper single slot grids, counterstained with Reynold's lead citrate, air-dried, and stored in grid boxes until EM observations.

Double immune-EM procedures to localize PHAL and CaMKIIα.—The following procedure was used to localize both PHAL and CaMKIIα immunoreactivity in the same sections. After the sodium borohydride and cryoprotectant steps described above, sections were pre-incubated in a PBS solution containing 5% milk for 30 min, rinsed in TBS-gelatin (pH 7.6; 3 × 5 min), and incubated overnight in a TBS-gelatin solution containing 1% milk, mouse anti-CaMKII (1:4000, Abcam, Cambridge, MA) and rabbit anti-PHAL antibodies (1:1000, Vector Labs, Burlingame, CA). Sections were next rinsed in TBS-Gelatin (3 × 10 min) and incubated for 2 hours in gold-conjugated goat anti-mouse IgGs (1:100, catalog # 2002, lot # 32C677, RRID AB_2637031, Nanogold, Nanoprobes, Stonybrook, NY) and in biotinylated goat anti-rabbit IgGs (1:200, Vector Laboratories, Burlingame, CA) in a TBS-gelatin solution containing 1% milk. Sections were next rinsed with TBS-gelatin (2 × 10 min) and a 2% aqueous acetate buffer solution (pH 7.0) for 10 min and then transferred to a darkroom for silver intensification of gold particles for 8-10 min using the HQ silver kit (Nanoprobes, Stonybrook, NY). After intensification, sections were rinsed repeatedly in acetate buffer and in TBS-gelatin for 10 min. They were then incubated with the ABC solution in TBS-gelatin with 1% milk for 90 min, rinsed in TBS-gelatin (2 × 10 min) and in

Tris buffer for 10 min. Last, sections were incubated in DAB (0.025%) for 10 min at room temperature, rinsed thoroughly in PBS, and transferred in 0.1M PB (pH 7.4) for 5 min. The remaining steps were as described above with the exception that we used 0.5% osmium tetroxide for 10 min and uranyl acetate for 10 min.

First, slides prepared for light microscopy were examined in order to determine the location of the PHAL injections in each animal. Only tissue from animals with injection sites restricted to the targeted locations (CMT and PVT) were included in the data analysis. For each successful PHAL injection site, two to four blocks of tissue were examined in each region of interest, depending on the density of labeled terminals that could be analyzed per blocks. Selected sections were photographed and the area of interest was drawn on the photographs. The tissue blocks were then cut in 70 nm-thick sections that were collected onto copper single slot grids. Only the most superficial ultrathin sections of the blocks were considered to ensure optimal penetration of the antibodies. Grids were examined in a transmission electron microscope (100 kV; magnification 10,000 to 60,000; JEM-1011, JEOL, Peabody, MA) and micrographs were digitally imaged by an 11 Megapixel lens-coupled CCD camera (ES1000W, Gatan, Warrendale, PA). The observer was blind to the location of the PHAL injection sites and the source of the tissue blocks used for EM observations.

Controls for single and double immunostaining reaction.—To control for the specificity of the PHAL reaction, some sections at the level of the injection sites and BL were incubated with solutions from which the primary rabbit anti-PHAL antibody was omitted, while the rest of the procedure remained the same. These sections were completely devoid of peroxidase labeling.

To control for the specificity of the double-labeling procedure (PHAL/CAMKIIα), each primary antibody was omitted in turn from the immunohistochemical reaction. Control sections incubated in solutions that did not contain the PHAL antibody were devoid of any peroxidase labeling, whereas omission of the CAMKIIα antibody from the incubation solutions let to a complete lack of gold labeling over the tissue.

Data analysis

Sections were searched systematically for PHAL-labeled axon terminals forming clear synapses with easily identifiable postsynaptic elements. The presence of the amorphous electron dense peroxidase reaction product was used to identify PHAL-labeled axon terminals. Postsynaptic elements were categorized using the ultrastructural criteria defined by Peters, Palay, & Webster (1991), as detailed in the Results section.

We performed EM observations on tissue processed to reveal either PHAL or PHAL and CaMKIIα immunoreactivity. In the latter case, CaMKIIα was revealed using the pre-embedding immunogold-silver intensification procedure. However, because this method only allows to assess CaMKIIα immunoreactivity in the most superficial ultrathin sections, we lumped deeper PHAL-labeled terminals found in areas devoid of CaMKIIα immunoreactivity with those sampled in tissue processed to reveal PHAL only.

Digital photomicrographs of labeled axon terminals were cropped into Adobe Photoshop CS5 (Adobe Systems Incorporated, San Jose, CA). Brightness and contrast adjustments were applied to the entire image using the same software. The photographs were then imported in Adobe Illustrator CS5 to add labels and scale bars.

RESULTS

Light microscopic observations

A total of 18 rats received iontophoretic PHAL injections in the CMT (n=8) or PVT (n=10), respectively. While a few nearby midline dorsal thalamic nuclei (rhomboid, parataenial, and reuniens) also project to the amygdala, prior tracing studies have revealed that they contribute only minor inputs to BL compared to CMT and PVT (Ruschen, 1982; Turner & Herkenham, 1991; Vertes, Hoover, Do Valle, Sherman, & Rodriguez, 2006; Vertes & Hoover, 2008; Vertes, Hoover, & Rodriguez, 2012). Nevertheless, to minimize contamination of our results by these other midline thalamic inputs, we restricted our EM analyses to a subset of rats in which nearly all PHAL-labeled somata were located within CMT (n=5; Fig. 1a,b) or PVT (n=3; Fig. 2a,b). Note that while the PHAL injection sites in PVT often encroached on the mediodorsal thalamic nucleus and habenula, to the best of our knowledge these nuclei do not project to BL (reviewed in Amaral, Price, Pitkanen, & Carmichael, 1992; Pitkanen, 2000).

Consistent with prior reports (Turner & Herkenham, 1991; Vertes, Hoover, Do Valle, Sherman, & Rodriguez, 2006; Vertes & Hoover, 2008; Vertes, Hoover, & Rodriguez, 2012), the pattern of anterograde labeling observed following PHAL injections in CMT and PVT differed markedly. Whereas CMT inputs to the amygdala were mostly confined to BL (Fig. 1d-f), PVT axons heavily targeted both BL and CeA (Fig. 2d-f). The density of anterogradely labeled axons in BL was higher after PHAL injections in CMT (Fig. 1d-f) than PVT (Fig. 2d-f). After PVT injections, the density of PHAL-labeled axons was markedly higher caudally than rostrally. In contrast, CMT axons had a relatively uniform distribution throughout BL. At high magnification, CMT and PVT axons in BL and CeA could be seen to contribute numerous *en passant* axonal varicosities (Fig. 1c, Fig. 2c).

Electron microscopic observations

We first describe the results obtained in BL, using tissue processed to reveal only PHAL immunoreactivity. PHAL-positive elements could be easily identified because they contained the electron-dense amorphous DAB reaction product. A total of 241 CMT (Fig. 3) and 93 PVT (Fig. 4) PHAL-positive axon terminals forming clear synapses were observed in BL. These samples were obtained in roughly equal proportions across the five CMT and three PVT rats (range: CMT, 39-63 terminals/rat; PVT, 22-41 terminals/rat).

Similar results were obtained following PHAL injections in CMT or PVT. With one exception (Fig. 4f), all PHAL-positive CMT and PVT axon terminals formed asymmetric synapses with their targets (Table 1) and displayed similar ultrastructural features including an overlapping range of cross-sectional diameters (CMT, 210-1800 nm; PVT, 220-1600 nm), the presence of a few mitochondria and of densely packed, round electron-lucent synaptic

vesicles. Another common feature was the relative incidence of the different types of post-synaptic elements. In both cases, axospinous synapses prevailed (CMT, 96.7%; PVT, 90.3%) followed by axodendritic synapses (CMT, 2.9%; PVT, 8.6%). In all PVT and CMT animals, dendritic spines outnumbered, by far, dendritic shafts as the type of element post-synaptic to PHAL-labeled axon terminals. The proportion of axospinous synapses were 95.2, 93.1, and 85.1% in the three PVT rats and 95.2, 93.8. 100, 94.7, and 100 % in the five CMT rats.

Figures 3 and 4 illustrate various examples of synapses formed by PHAL-labeled CMT and PVT axon terminals in BL, respectively. Figures 3a-h and 4a-d depict examples of synapses formed by PHAL-positive axon terminals with dendritic spines, recognized as such by the the lack of microtubules and mitochondria, coupled to the presence of a spine apparatus (Peters, Palay, & Webster, 1991). When the plane of the section was favorable, the spines could be seen to emerge from their parent dendrite (Fig. 3a,g). In other cases, only spine heads were present in the section (Fig. 4a-d), while in others, the spine neck was also visible (Fig. 3b,h). Although far less frequent, axodendritic synapses were easy to identify (Fig. 3i, 4e,f) because dendritic profiles were typically larger and contained various combinations of the following structures: microtubules, mitochondria, and endoplasmic reticulum (Peters, Palay, & Webster, 1991). Only one instance of axosomatic synapse was encountered, following a PHAL injection in CMT (Fig. 3j).

Synaptic relationships between PHAL-labeled terminals and CaMKIIα-immunoreactive BL neurons

The above results suggest that CMT and PVT axon terminals preferentially form excitatory synapses with dendritic spines, and less frequently with dendritic shafts. However, because BL contains multiple cell types, the identity of the neurons targeted by CMT and PVT inputs is unclear. As in the cerebral cortex, principal BL cells are glutamatergic neurons with spiny dendrites whereas interneurons are GABAergic and mostly devoid of dendritic spines (reviewed in McDonald, 1992; Spampanato, Polepalli, & Sah, 2011). As a result, it is generally assumed that, as in cortex (Colonnier, 1981; DeFelipe & Fariñas, 1992; Peters, Palay, & Webster, 1991), excitatory inputs to principal BL cells form asymmetric synapses with dendritic spines whereas asymmetric synapses on dendritic shafts represent excitatory inputs to local-circuit cells (Carlsen & Heimer, 1988; Muller, Mascagni, & McDonald, 2003, 2006, 2007; Paré, Smith, & Paré, 1995; Smith & Paré, 1994).

To verify whether this assumption is correct in the case of CMT and PVT inputs, we took advantage of the fact that, as in cortex (Benson, Isackson, Gall, & Jones, 1992; Tighilet, Hashikawa, & Jones, 1998; Unal, Paré, Smith, & Paré, 2013), immunoreactivity for CaMKIIα (Liu & Murray, 2012) is a specific marker of principal BL neurons (McDonald & Mascagni, 2010; McDonald, Muller, & Mascagni, 2002; Muller, Mascagni, & McDonald, 2007, 2009). Indeed, CaMKIIα immunoreactivity is found in their soma, proximal and distal dendrites, and in a proportion of their dendritic spines (McDonald, Muller, & Mascagni, 2002). In contrast, GABAergic interneurons of BL do not express CaMKIIα (McDonald & Mascagni, 2010; McDonald, Muller, & Mascagni, 2002; Muller, Mascagni, & McDonald, 2007, 2009). Thus, we sought to determine whether the targets of PHAL-positive CMT and PVT axon terminals were immunoreactive for CaMKIIα.

In these experiments, PHAL was detected with the same immunoperoxidase method as above and CAMKIIα immunoreactivity with the pre-embedding immunogold-silver intensification procedure. Only the most superficial ultrathin sections of the blocks were considered to ensure optimal penetration of the antibodies. In the electron microscope, CaMKIIα-positive elements were easily distinguishable by the presence of numerous gold particles. To avoid false-positive results due to non-specific gold labeling, dendritic profiles and somata had to contain at least three gold particles to be categorized as immunoreactive. In the case of dendritic spines, a prior report indicated that they do not consistently display CaMKIIα-immunoreactivity (McDonald, Muller, & Mascagni, 2002). Thus, lack of immunoreactivity for CaMKIIα by a dendritic spine was not interpreted as evidence that the post-synaptic target was an interneuron unless the spine could be seen to emerge from a dendrite that was also CaMKIIα immunonegative.

In ultrathin sections considered appropriate to assess CaMKIIα immunoreactivity, a total of 162 CMT (Fig. 5) and 126 (Fig. 6) PVT axon terminals forming clear synapses were observed. All of these terminals formed asymmetric synapses, usually with dendritic spines (CMT, 96.9% or 157 of 162; PVT; 91.2% or 115 of 126), but occasionally with dendritic profiles (CMT, 3.1% or 5 of 162; PVT, 8.7% or 11 of 126). In all cases where CaMKIIα immunonegative spines could be seen to emerge from their parent dendrite (CMT, n=5; PVT, n=5), the latter was immunopositive for CaMKIIα (Figs. 5a-d and 6a-e). With respect to axo-dendritic synapses, all dendritic profiles contacted by CMT axon terminals (n=5) were CaMKIIα positive (Fig. 5e-h), while 72.7% of dendrites (n=11) contacted by PVT axon terminals were immunoreactive for CaMKIIα (Fig. 6f-g). Figure 6h depicts a rare example of PVT axon terminal forming an asymmetric synapse with a CaMKIIα-negative dendrite.

Of note, in a substantial proportion of synapses formed by PVT (22.4%) and CMT (29.8%) axon terminals, the active zone was discontinuous. Examples of such synapses can be seen in figures 4a,c,d and 5d,g for PVT and CMT, respectively. While these may represent so-called perforated synapses, confirmation that this is the case awaits EM examination of serial ultrathin sections.

Synaptic relationships between PHAL-labeled terminals and CeA neurons

For comparison, we also determined the postsynaptic targets of PVT axon terminals ending in CeA, particularly in its lateral sector (CeL) where PVT inputs were concentrated. Note that unlike BL, whose cytoarchitecture is reminiscent of cortex (Calsen & Heimer, 1988), that of CeL is akin to the striatum, including a dominant cell type whose morphological features are identical to that of medium spiny striatal neurons and a major input from midbrain dopaminergic cell groups (McDonald, 1982, 1992; Swanson & Petrovich, 1998). Thus, it is likely that as in the striatum, local-circuit cells account for a minute (~1%) proportion of CeA neurons (Tepper & Bolam, 2004). Moreover, since projection cells and interneurons are GABAergic in CeA, CaMKIIα is not a useful marker to distinguish these two CeA cell types.

A total of 99 PVT (Fig. 7) PHAL-positive axon terminals forming clear synapses were observed in CeA. This data was obtained in two rats (66 and 33 synapses, respectively). The quality of the ultrastructure proved insufficient for EM observations in the third PVT animal.

Similar to our observations in BL, the vast majority (96.9%) of PHAL-positive PVT axon terminals formed asymmetric synapses with their targets. Their ultrastructural features were indistinguishable from those of PVT axon terminals in BL, including the presence of mitochondria and of densely packed, round electron-lucent synaptic vesicles. Also as in BL, axospinous synapses prevailed (89.9%; Fig. 7a,b) followed by axodendritic synapses (7.1%; Fig. 7c) and no axosomatic synapses were observed. In one rat, we found three PHAL-positive PVT axon terminals formed symmetric synapses with dendritic profiles (3%; Fig. 7d). It should be noted that symmetric synapses are difficult to identify unambiguously, especially when the presynaptic element is intensely labeled with DAB. Moreover, because we did not observe synapses through serial ultrathin sections, we cannot exclude the possibility that in these rare cases of symmetric synapses, the postsynaptic density would have been thicker in adjacent sections.

DISCUSSION

CMT and PVT are major sources of subcortical inputs to BL (Turner & Herkenham, 1991; Vertes & Hoover, 2008; Vertes, Hoover, & Rodriguez, 2012), raising the possibility that they exert a profound influence over BL activity. However, a deeper understanding of the synaptic microcircuits through which these thalamic inputs mediate their effects is essential to elucidate their potential role in shaping BL activity. Thus, using a combination of electron microscopy, tracttracing, and immunocytochemistry, we examined the ultrastructural properties and synaptic targets of CMT and PVT axon terminals and found that most of them formed asymmetric axospinous synapses with principal BL cells. Although a substantial proportion of CMT and PVT axon terminals formed axodendritic synapses, most of these dendrites also belonged to principal BL cells, thereby suggesting that CMT and PVT neurons are heavily connected with principal BL neurons, but not much with GABAergic interneurons. Below, we consider the significance of these results in light of prior studies about the ultrastructure, connectivity, and physiology of thalamic inputs to the amygdala.

Comparison with prior studies on thalamic inputs to the amygdala

Most prior studies of thalamo-amygdala relations have focused on inputs from the medial portion of the medial geniculate nucleus (MGMm) to the lateral amygdala (LA) because of their involvement in auditory fear conditioning (LeDoux, 2000; McKernan & Shinnick-Gallagher, 1997; Rogan & LeDoux, 1995; Rumpel, LeDoux, Zador, & Malinow, 2005). MGMm neurons that innervate LA are glutamatergic, as shown by the blockade of LA responses to MGMm inputs by glutamate receptor antagonists (Li, Phillips, & LeDoux, 1995) and the expression of glutamate receptor subunits postsynaptic to MGMm axon terminals (Farb & LeDoux, 1997; Humeau et al., 2005; Radley et al., 2007). Consistent with this, MGMm axon terminals exclusively form asymmetric synapses in LA, most frequently with the dendritic spines of principal cells, but also, in ~30% of cases, with dendritic profiles (LeDoux, Farb, & Milner, 1991), some of which were positively identified as belonging to interneurons (Woodson, Farb, & LeDoux, 2000).

In contrast with MGMm, the transmitter used by CMT and PVT neurons has not been formally identified. However, the near total absence of GABAergic neurons in the dorsal thalamus of the rat (Houser, Vaughn, Barber, & Roberts, 1980) suggests that they too are glutamatergic. Supporting this possibility, we found that the ultrastructural features of CMT and PVT axon terminals in BL are similar to those of MGMm terminals in LA. That is, CMT and PVT axon terminals are small- to medium-sized, packed with electron-lucent vesicles, and form asymmetric synapses, mostly with dendritic spines and, in ~3-9% of cases, with dendritic shafts. This proportion of axodendritic synapses is markedly lower than that reported for MGMm inputs to LA (LeDoux, Farb, & Milner, 1991), suggesting a differential involvement of GABAergic interneurons in mediating feed-forward inhibition in response to MGMm vs. CMT/PVT thalamic drive of the amygdala.

Because local-circuit cells in BL and the cerebral cortex are aspiny or sparsely spiny (Colonnier, 1981; DeFelipe & Fariñas, 1992; McDonald, 1992; Peters, Palay, & Webster, 1991; Spampanato, Polepalli, & Sah, 2011), axodendritic asymmetric synapses have generally been assumed to represent excitatory synapses onto inhibitory interneurons (Muller, Mascagni, & McDonald, 2003, 2006, 2007; Paré, Smith, & Paré, 1995; Smith & Paré, 1994). In prior studies, a majority of cortical (Brinley-Reed, Mascagni, & McDonald, 1995; Smith, Paré, & Paré, 2000), MGMm (LeDoux, Farb, & Milner, 1991), and intrinsic (Smith & Paré, 1994; Smith, Paré, & Paré, 2000) axon terminals to the basolateral amygdaloid complex were found to contact dendritic spines. Most of these studies reported that axodendritic synapses accounted for only 3-10% of synapses, MGMm inputs to LA being the sole exception with ~30% targeting dendritic shafts. In the few studies that attempted to identify the targets of these axodendritic synapses, calbindin (Unal, Paré, Smith, & Paré, 2014) but not pavalbumin (Smith, Paré, & Paré, 2000) positive interneurons were found to receive cortical inputs, whereas parvalbumin interneurons constituted a major target of intrinsic glutamatergic synapses (Smith, Paré, & Paré, 2000).

In contrast with these prior findings, we found that most of the dendritic shafts contacted by CMT and PVT axon terminals are immunoreactive for CaMKIIα, a selective marker of principal cells in BL (McDonald & Mascagni, 2010; McDonald, Muller, & Mascagni, 2002; Muller, Mascagni, & McDonald, 2007, 2009). Together, these observations suggest that CMT and PVT inputs to BL are largely directed to principal cells such that when CMT or PVT neurons fire, little feed-forward inhibition counters their excitatory influence on principal neurons. Assuming that thalamic synapses in BL are as strong as in the cerebral cortex, such that activation of one or just a few thalamic synapses is sufficient to fire postsynaptic cells (Ahmed, Anderson, Douglas, Martin, & Whitteridge, 1998; Bannister, Nelson, & Jack, 2002; Douglas & Martin, 1991; Swadlow, Gusev, & Bezdudnaya, 2002), these results would imply that CMT and PVT inputs constitute a major determinant of BL activity.

Our results are also consistent with a prior study on the innervation of BL by the interanteromedial (IAM) thalamic nucleus (Calrsen & Heimer, 1988). This study reported that nearly all (>99%) PHAL-labeled IAM axon terminals ending in BL form axospinous synapses. Additional experiments combining IAM lesions with Golgi impregnation of BL

neurons confirmed that the spines post-synaptic to IAM axon terminals belonged to principal BL neurons.

Nature of signals conveyed by BL-projecting PVT and CMT neurons

It has long been recognized that BL neurons are responsive to various types of sensory stimuli, particularly if they have been paired with aversive or rewarding outcomes (for instance see Uwano, Nishijo, Ono, & Tamura, 1995). In fact, recent studies have revealed that BL neurons concurrently encode multiple dimensions, including the sensory properties of stimuli, their reward value, contextual information, the hierarchical rank of con-specifics as well as various behaviors such as freezing, active avoidance, reward approach, and movement speed (Amir, Lee, Headley, Herzallah, & Paré, 2015; Belova, Paton, & Salzman, 2008; Kyriazi, Headley, & Paré, 2018; Munuera, Rigotti, & Salzman, 2018; Saez, Rigotti, Ostojic, Fusi, & Salzman, 2015).

At present the identity of the pathways conveying these various types of signals to BL is unclear. The potential contribution of CMT and PVT in particular is unknown because little singleunit data is available in these thalamic nuclei as most studies relied on the expression of immediate early genes (see references listed in the Introduction). Further complicating this issue is the fact that, BL, CMT and PVT share many inputs. For instance, the mPFC is a potential source of multimodal information to all three structures (Ongür & Price, 2000; Vertes, Linley, & Hoover, 2015). Yet, obvious similarities between the responsiveness of midline thalamic and BL neurons are consistent with the notion that PVT and CMT inputs determine, at least in part, the type of information encoded by BL neurons.

For instance, PVT and BL neurons are both responsive to emotionally arousing stimuli irrespective of valence (Vertes, Linley, & Hoover, 2015). In a fear conditioning paradigm, inhibition of PVT neurons reduces the expression of conditioned fear responses (Do-Monte, Quiñones-Laracuente, & Quirk, 2015; Padilla-Coreano, Do-Monte, & Quirk, 2012), suggesting that PVT relays information about conditioned stimuli to BL. Also, PVT receives significant inputs from the suprachiasmatic nucleus (Kawano, Krout, & Loewy, 2001), potentially explaining why BL shows a prominent circadian periodicity in the expression of the clock protein Period2 (Amir & Stewart, 2009).

Similarly, CMT inputs likely contribute to the response profile of BL neurons. Indeed, CMT is unusual among midline thalamic nuclei because it is connected with both limbic and sensorimotor structures (Vertes, Linley, & Hoover, 2015). Among the latter, the deep layers of the superior colliculus project to CMT, likely providing BL with multimodal sensory information, including visual, auditory and, somatosensory signals (Basso & May, 2017; Krout, Loewy, Westby, & Redgrave, 2001). Similarly, parabrachial inputs to CMT may contribute to the responsiveness of BL neurons to taste, noxious, and visceral stimuli (Krout & Loewy, 2000).

Conclusions

Overall, the present study indicates that midline thalamic inputs occupy an unusual position in the synaptic microcircuitry of the amygdala. Not only do they densely innervate BL

(Vertes, Linley, & Hoover, 2015), they also target almost exclusively principal cells, which distinguishes them from other glutamatergic afferents to BL (Brinley-Reed, Mascagni, & McDonald, 1995; Smith & Paré, 1994; Smith, Paré, & Paré, 2000; Stefanacci et al., 1992). A challenge for future studies will be to determine the functional significance of this differential synaptic connectivity and the type of information these thalamic inputs convey to BL neurons. In addition, further studies will be needed to better understand the relationships between thalamic inputs and specific subtypes of CeA neurons.

ACKNOWLEDGMENTS

This work was supported by R01 grant R01MH107239 to DP from NIMH and NIH/ORIP Yerkes Center base grant P51 OD011132 to YS.

LITERATURE CITED

Ahmed B, Anderson JC, Douglas RJ, Martin KA, & Whitteridge D (1998). Estimates of the net excitatory currents evoked by visual stimulation of identified neurons in cat visual cortex. Cereb Cortex, 8(5), 462–76. 10.1093/cercor/8.5.462 [PubMed: 9722089]

Alkire MT, McReynolds JR, Hahn EL, & Trivedi AN (2007). Thalamic microinjection of nicotine reverses sevoflurane-induced loss of righting reflex in the rat. Anesthesiology, 107(2), 264–272. 10.1097/01.anes.0000270741.33766.24 [PubMed: 17667571]

Amaral DG, Price JL, Pitkanen A, & Carmichael ST (1992). In Aggleton JP (Ed.), The amygdala: neurobiological aspects of emotion, memory, and mental dysfunction. (pp.1–66). New York, NY: Wiley-Liss.

Amir A, Lee SC, Headley DB, Herzallah MM, & Paré D (2015). Amygdala signaling during foraging in a hazardous environment. J Neurosci, 35(38), 12994–3005. 10.1523/jneurosci.0407-15.2015 [PubMed: 26400931]

Amir S, & Stewart J (2009). Motivational modulation of rhythms of the expression of the clock protein PER2 in the limbic forebrain. Biol Psychiatry, 65(10), 829–34. 10.1016/j.biopsych.2008.12.019 [PubMed: 19200536]

Baker R, Gent TC, Yang Q, Parker S, Vyssotski AL, Wisden W,…Franks NP (2014).Altered activity in the central medial thalamus precedes changes in the neocortex during transitions into both sleep and propofol anesthesia. J Neurosci, 34(40), 13326–35. 10.3410/f.719128663.793513279 [PubMed: 25274812]

Bannister NJ, Nelson JC, & Jack JJ (2002). Excitatory inputs to spiny cells in layers 4 and 6 of cat striate cortex. Philos Trans R Soc Lond B Biol Sci, 357(1428), 1793–808. 10.3410/f.1012685.186635 [PubMed: 12626013]

Basso MA, & May PJ (2017). Circuits for Action and Cognition: A View from the Superior Colliculus. Annu Rev Vis Sci, 3, 197–226. 10.1146/annurev-vision-102016-061234 [PubMed: 28617660]

Belova MA, Paton JJ, & Salzman CD (2008). Moment-to-moment tracking of state value in the amygdala. J Neurosci, 28(40), 10023–30. 10.1523/jneurosci.1400-08.2008 [PubMed: 18829960]

Benson DL, Isackson PJ, Gall CM, & Jones EG (1992). Contrasting patterns in the localization of glutamic acid decarboxylase and Ca2+/calmodulin protein kinase gene expression in the rat central nervous system. Neuroscience, 46(4), 825–849. 10.1016/0306-4522(92)90188-8 [PubMed: 1311814]

Benarroch EE (2008). The midline and intralaminar thalamic nuclei: anatomic and functional specificity and implications in neurologic disease. Neurology, 71(12), 944–9. 10.1212/01.wnl.0000326066.57313.13 [PubMed: 18794498]

Brinley-Reed M, Mascagni F, & McDonald AJ (1995). Synaptology of prefrontal cortical projections to the basolateral amygdala: an electron microscopic study in the rat. Neurosci Lett, 202(1–2), 45–8. 10.1016/0304-3940(95)12212-5 [PubMed: 8787827]

Brown EE, Robertson GS, & Fibiger HC (1992). Evidence for conditional neuronal activation following exposure to a cocaine-paired environment: role of forebrain limbic structures. J Neurosci, 12(10), 4112–21. 10.1523/jneurosci.12-10-04112.1992 [PubMed: 1403102]

Bubser M, & Deutch AY (1999). Stress induces Fos expression in neurons of the thalamic paraventricular nucleus that innervate limbic forebrain sites. Synapse, 32(1), 13–22. 10.1002/(sici)1098-2396(199904)32:1<13::aid-syn2>3.0.co;2-r [PubMed: 10188633]

Carlsen J, & Heimer L (1988). The basolateral amygdaloid complex as a cortical-like structure. Brain Res, 441(1–2), 377–380. 10.1016/0006-8993(88)91418-7 [PubMed: 2451985]

Colonnier M (1981). The electron-microscopic analysis of the neuronal organization of the cerebral cortex In Schmitt FO, Worden FG, Adelman G, Dennis SG (Eds.). The organization of the cerebral cortex (pp. 125–152). Cambridge, MA: MIT Press.

DeFelipe J, & Fariñas I (1992). The pyramidal neuron of the cerebral cortex: morphological and chemical characteristics of the synaptic inputs. Prog Neurobiol, 39(6), 563–607. 10.1016/0301-0082(92)90015-7 [PubMed: 1410442]

Deutch AY, Bubser M, & Young CD (1998). Psychostimulant-induced Fos protein expression in the thalamic paraventricular nucleus. J Neurosci, 18(24), 10680–7. 10.1523/jneurosci.18-24-10680.1998 [PubMed: 9852603]

Do-Monte FH, Quiñones-Laracuente K, & Quirk GJ (2015). A temporal shift in the circuits mediating retrieval of fear memory. Nature, 519(7544), 460–3. 10.1038/nature14030 [PubMed: 25600268]

Douglas RJ, & Martin KA (1991). A functional microcircuit for cat visual cortex. J Physiol, 440, 735–69. 10.1113/jphysiol.1991.sp018733 [PubMed: 1666655]

Erondu NE, & Kennedy MB (1985). Regional distribution of type II Ca2+/calmodulin-dependent protein kinase in rat brain. J Neurosci, 5(12), 3270–3277. 10.1523/jneurosci.05-12-03270.1985 [PubMed: 4078628]

Farb CR, & LeDoux JE (1997). NMDA and AMPA receptors in the lateral nucleus of the amygdala are postsynaptic to auditory thalamic afferents. Synapse, 27(2), 106–21. 10.1002/(SICI)1098-2396(199710)27:2<106::AID-SYN2>3.0.CO;2-I [PubMed: 9266772]

Franklin TR, & Druhan JP (2000). Expression of Fos-related antigens in the nucleus accumbens and associated regions following exposure to a cocaine-paired environment. Eur J Neurosci, 12(6), 2097–106. 10.1046/j.1460-9568.2000.00071.x [PubMed: 10886349]

Hall E (1972). The amygdala of the cat: a Golgi study. Z Zekkforsch Mikrosk Anat, 134(4), 439–58.

Houser CR, Vaughn JE, Barber RP, & Roberts E (1980). GABA neurons are the major cell type of the nucleus reticularis thalami. Brain Res, 200(2), 341–54. 10.1016/0006-8993(80)90925-7 [PubMed: 7417821]

Humeau Y, Herry C, Kemp N, Shaban H, Fourcaudot E, Bissière S, & Lüthi A (2005). Dendritic spine heterogeneity determines afferent-specific Hebbian plasticity in the amygdala. Neuron, 45(1), 119–31. 10.1016/j.neuron.2004.12.019 [PubMed: 15629707]

Igelstrom KM, Herbison AE, & Hyland BI (2010). Enhanced c-Fos expression in superior colliculus, paraventricular thalamus and septum during learning of cue-reward association. Neuroscience, 168(3), 706–14. 10.1016/j.neuroscience.2010.04.018 [PubMed: 20399252]

Johnson ZV, Revis AA, Burdick MA, & Rhodes JS (2010). A similar pattern of neuronal Fos activation in 10 brain regions following exposure to reward- or aversion-associated contextual cues in mice. Physiol Behav, 99(3), 412–8. 10.1016/j.physbeh.2009.12.013 [PubMed: 20026143]

Jones EG (2007). The Thalamus (Second edition) Cambridge: Cambridge University Press.

Jung SC, Kim J, & Hoffman DA (2008). Rapid, bidirectional remodeling of synaptic NMDA receptor subunit composition by A-type K channel activity in hippocampal CA1 pyramidal neurons. Neuron, 60(4), 657–671. 10.1016/j.neuron.2008.08.029 [PubMed: 19038222]

Kawano J, Krout KE, & Loewy AD (2001). Suprachiasmatic nucleus projections to the paraventricular thalamic nucleus of the rat. Thal Rel Syst, 1, 197–202. 10.1016/s1472-9288(01)00019-x

Krettek JE, & Price JL (1977). Projections from the amygdaloid complex to the cerebral cortex and thalamus in the rat and cat. J Comp Neurol, 172(4), 687–722. 10.1002/cne.901720408 [PubMed: 838895]

Krout KE, & Loewy AD (2000). Parabrachial nucleus projections to midline and intralaminar thalamic nuclei of the rat. J Comp Neurol, 428(3), 475–494. 10.1002/1096-9861(20001218)428:3<475::aid-cne6>3.0.co;2-9 [PubMed: 11074446]

Krout KE, Loewy AD, Westby GW, & Redgrave P (2001). Superior colliculus projections to midline and intralaminar thalamic nuclei of the rat. J Comp Neurol, 431(2), 198–216. 10.1002/1096-9861(20010305)431:2<198::aid-cne1065>3.0.co;2-8 [PubMed: 11170000]

Kuroda R, Yorimae A, Yamada Y, Furuta Y, & Kim A (1995). Frontal cingulotomy reconsidered from a WGA-HRP and c-Fos study in the cat. Acta Neurochir, 64, 69–73. 10.1007/978-3-7091-9419-5_15

Kyriazi P, Headley DB, & Paré D (2018). Multi-dimensional coding by basolateral amygdala neurons. Neuron, 99, 1–14. 10.1016/j.neuron.2018.07.036 [PubMed: 30001504]

LeDoux JE (2000). Emotion circuits in the brain. Annu Rev Neurosci, 23, 155–184. 10.1146/annurev.neuro.23.1.155 [PubMed: 10845062]

LeDoux JE, Farb CR, & Milner TA (1991). Ultrastructure and synaptic associations of auditory thalamo-amygdala projections in the rat. Exp Brain Res, 85(3), 577–86. 10.1007/bf00231742 [PubMed: 1717305]

Leung LS, Luo T, Ma J, & Herrick I (2014). Brain areas that influence general anesthesia. Prog Neurobiol, 122, 24–44. 10.1016/j.pneurobio.2014.08.001 [PubMed: 25172271]

Li XF, Phillips R, & LeDoux JE (1995). NMDA and non-NMDA receptors contribute to synaptic transmission between the medial geniculate body and the lateral nucleus of the amygdala. Exp Brain Res, 105(1), 87–100. 10.1007/bf00242185 [PubMed: 7589322]

Liu XB, & Murray KD (2012). Neuronal excitability and calcium/calmodulin-dependent protein kinase type II: location, location, location. Epilepsia 53, Suppl 1, 45–52. 10.1111/j.1528-1167.2012.03474.x.

Lkhagvasuren B, Oka T, Nakamura Y, Hayashi H, Sudo N, & Nakamura K (2014).Distribution of Fos-immunoreactive cells in rat forebrain and midbrain following social defeat stress and diazepam treatment. Neuroscience, 272, 34–57. 10.1016/j.neuroscience.2014.04.047 [PubMed: 24797330]

McDonald AJ (1982). Cytoarchitecture of the central amygdaloid nucleus of the rat. J Comp Neurol, 208(4), 401–18. 10.1002/cne.902080409 [PubMed: 7119168]

McDonald AJ (1992). Cell types and intrinsic connections of the amygdala In Aggleton JP (Ed.), The amygdala: neurobiological aspects of emotion, memory, and mental dysfunction. (pp.67–96). New York, NY: Wiley-Liss.

McDonald AJ, Muller JF, & Mascagni F (2002). GABAergic innervation of alpha type II calcium/calmodulin-dependent protein kinase immunoreactive pyramidal neurons in the rat basolateral amygdala. J Comp Neurol, 446(3), 199–218. 10.1002/cne.10204 [PubMed: 11932937]

McDonald AJ, & Mascagni F (2010). Neuronal localization of m1 muscarinic receptor immunoreactivity in the rat basolateral amygdala. Brain Struct Funct, 215(1), 37–48. 10.1007/s00429-010-0272-y [PubMed: 20503057]

McKenna JE, & Melzak R (1994). Dissociable effects of lidocaine injection into the medial versus lateral thalamus in tail-flick and formalin pain tests. Pathophysiology, 1, 205–214. 10.1016/0928-4680(94)90039-6

McKernan MG, & Shinnick-Gallagher P (1997). Fear conditioning induces a lasting potentiation of synaptic currents in vitro. Nature, 390(6660), 607–11. 10.1038/37605 [PubMed: 9403689]

Muller JF, Mascagni F, & McDonald AJ (2003). Synaptic connections of distinct interneuronal subpopulations in the rat basolateral amygdalar nucleus. J Comp Neurol, 456(3), 217–236. 10.1002/cne.10435 [PubMed: 12528187]

Muller JF, Mascagni F, & McDonald AJ (2006). Pyramidal cells of the rat basolateral amygdala: synaptology and innervation by parvalbumin immunoreactive interneurons. J Comp Neurol, 494(4), 635–650. 10.1002/cne.20832 [PubMed: 16374802]

Muller JF, Mascagni F, & McDonald AJ (2007). Postsynaptic targets of somatostatin-containing interneurons in the rat basolateral amygdala. J Comp Neurol, 500(3), 513–529. 10.1002/cne.21185 [PubMed: 17120289]

Muller JF, Mascagni F, & McDonald AJ (2009). Dopaminergic innervation of pyramidal cells in the rat basolateral amygdala. Brain Struct Funct, 213(3), 275–88. 10.1007/s00429-008-0196-y [PubMed: 18839210]

Munuera J, Rigotti M, & Salzman CD (2018). Shared neural coding for social hierarchy and reward value in primate amygdala. Nat Neurosci, 21(3), 415–423. 10.1038/s41593-018-0082-8 [PubMed: 29459764]

Ongür D, & Price JL (2000). The organization of networks within the orbital and medial prefrontal cortex of rats, monkeys and humans. Cereb Cortex, 10(3), 206–19. 10.1093/cercor/10.3.206 [PubMed: 10731217]

Otake K, Kin K, & Nakamura Y (2002). Fos expression in afferents to the rat midline thalamus following immobilization stress. Neurosci Res, 43(3), 269–82. 10.1016/s0168-0102(02)00042-1 [PubMed: 12103445]

Padilla-Coreano N, Do-Monte FH, & Quirk GJ (2012). A time-dependent role of midline thalamic nuclei in the retrieval of fear memory. Neuropharmacology, 62(1), 457–63. 10.1016/j.neuropharm.2011.08.037 [PubMed: 21903111]

Paré D, Smith Y, & Paré JF (1995). Intra-amygdaloid projections of the basolateral and basomedial nuclei in the cat: Phaseolus vulgaris leucoagglutinin anterograde tracing at the light and electron microscopic level. Neuroscience, 69(2), 567–583. 10.1016/0306-4522(95)00272-k [PubMed: 8552250]

Paxinos G, & Watson C (2007). The rat brain in stereotaxic coordinates. New York, NY: Academic Press.

Peters A, Palay SL, & Webster HF (1991). The fine structure of the nervous system. New York, NY: Oxford University Press.

Pitkanen A (2000). Connectivity of the rat amygdaloid complex In: Aggleton JP (Ed.), The amygdala: a functional analysis (pp. 31–116). Oxford, UK: Oxford University Press.

Price JL, & Drevets WC (2010). Neurocircuitry of mood disorders. Neuropsychopharmacology, 35(1), 192–216. 10.1038/npp.2009.104 [PubMed: 19693001]

Radley JJ, Farb CR, He Y, Janssen WG, Rodrigues SM, Johnson LR,…Morrison JH (2007). Distribution of NMDA and AMPA receptor subunits at thalamo-amygdaloid dendritic spines. Brain Res, 1134(1), 87–94. 10.1016/j.brainres.2006.11.045 [PubMed: 17207780]

Rogan MT, & LeDoux JE (1995). LTP is accompanied by commensurate enhancement of auditory-evoked responses in a fear conditioning circuit. Neuron, 15(1), 127–36. 10.1016/0896-6273(95)90070-5 [PubMed: 7619517]

Rumpel S, LeDoux J, Zador A, & Malinow R (2005). Postsynaptic receptor trafficking underlying a form of associative learning. Science, 308(5718), 83–8. 10.1126/science.1103944 [PubMed: 15746389]

Russchen FT (1982). Amygdalopetal projections in the cat. II. Subcortical afferent connections.A study with retrograde tracing techniques. J Comp Neurol, 207(2), 157–76. 10.1002/cne.902070205 [PubMed: 7096644]

Saez A, Rigotti M, Ostojic S, Fusi S, & Salzman CD (2015). Abstract context representations in primate amygdala and prefrontal cortex. Neuron, 87(4), 869–81. 10.1016/j.neuron.2015.07.024 [PubMed: 26291167]

Smith Y, & Paré D (1994). Intra-amygdaloid projections of the lateral nucleus in the cat: PHA-L anterograde labeling combined with post-embedding GABA and glutamate immunocytochemistry. J Comp Neurol, 342(2), 232–248. 10.1002/cne.903420207 [PubMed: 7911130]

Smith Y, Paré JF, & Paré D (2000). Differential innervation of parvalbumin-immunoreactive interneurons of the basolateral amygdaloid complex by cortical and intrinsic inputs. J Comp Neurol, 416(4), 496–508. 10.1002/(sici)1096-9861(20000124)416:4<496::aid-cne6>3.3.co;2-e [PubMed: 10660880]

Spampanato J, Polepalli J, & Sah P (2011). Interneurons in the basolateral amygdala. Neuropharmacology, 60(5), 765–773. 10.1016/j.neuropharm.2010.11.006 [PubMed: 21093462]

Spencer SJ, Fox JC, & Day TA (2004). Thalamic paraventricular nucleus lesions facilitate central amygdala neuronal responses to acute psychological stress. Brain Res, 997(2), 234–7. 10.1016/j.brainres.2003.10.054 [PubMed: 14706875]

Stefanacci L, Farb CR, Pitkänen A, Go G, LeDoux JE, & Amaral DG (1992).Projections from the lateral nucleus to the basal nucleus of the amygdala: a light and electron microscopic PHA-L study in the rat. J Comp Neurol, 323(4), 586–601. 10.1002/cne.903230411 [PubMed: 1430325]

Swadlow HA, Gusev AG, & Bezdudnaya T (2002). Activation of a cortical column by a thalamocortical impulse. J Neurosci, 22(17), 7766–73. 10.3410/f.1000417.179469 [PubMed: 12196600]

Swanson LW, & Petrovich GD (1998). What is the amygdala? Trends Neurosci, 21(8), 323–331. 10.1016/S0166-2236(98)01265-X [PubMed: 9720596]

Tepper JM, & Bolam JP (2004). Functional diversity and specificity of neostriatal interneurons. Curr Opin Neurobiol, 14(6), 685–692. 10.1016/j.conb.2004.10.003 [PubMed: 15582369]

Tighilet B, Hashikawa T, & Jones EG (1998). Cell- and lamina-specific expression and activity-dependent regulation of type II calcium/calmodulin-dependent protein kinase isoforms in monkey visual cortex. J Neurosci, 18(6), 2129–2146. 10.1523/jneurosci.18-06-02129.1998 [PubMed: 9482799]

Timofeeva E, & Richard D (2001). Activation of the central nervous system in obese Zucker rats during food deprivation. J Comp Neurol, 441(1), 71–89. 10.1002/cne.1398 [PubMed: 11745636]

Turner BH, & Herkenham M (1991). Thalamoamygdaloid projections in the rat: A test of the amygdala's role in sensory processing. J Comp Neurol, 313(2), 295–325. 10.1002/cne.903130208 [PubMed: 1765584]

Unal G, Paré JF, Smith Y, & Paré D (2013). Differential connectivity of short- vs. long-range extrinsic and intrinsic cortical inputs to perirhinal neurons. J Comp Neurol, 521(11), 2538–50. 10.1002/cne.23297 [PubMed: 23296922]

Unal G, Paré JF, Smith Y, & Paré D (2014). Cortical inputs innervate calbindin-immunoreactive interneurons of the rat basolateral amygdaloid complex. J Comp Neurol, 522(8), 1915–28. 10.1002/cne.23511 [PubMed: 24285470]

Uwano T, Nishijo H, Ono T, & Tamura R (1995). Neuronal responsiveness to various sensory stimuli, and associative learning in the rat amygdala. Neuroscience, 68(2), 339–61. 10.1016/0306-4522(95)00125-3 [PubMed: 7477945]

Van der Werf YD, Witter MP, & Groenewegen HJ (2002). The intralaminar and midline nuclei of the thalamus. Anatomical and functional evidence for participation in processes of arousal and awareness. Brain Res Reviews, 39(2–3), 107–140. 10.1016/s0165-0173(02)00181-9

Vertes RP, Hoover WB, Do Valle AC, Sherman A, & Rodriguez JJ (2006). Efferent projections of reuniens and rhomboid nuclei of the thalamus in the rat. J Comp Neurol, 499(5), 768–96. 10.1002/cne.21135 [PubMed: 17048232]

Vertes RP, & Hoover WB (2008). Projections of the paraventricular and paratenial nuclei of the dorsal midline thalamus in the rat. J Comp Neurol, 508(2), 212–37. 10.1002/cne.21679 [PubMed: 18311787]

Vertes RP, Hoover WB, & Rodriguez JJ (2012). Projections of the central medial nucleus of the thalamus in the rat: node in cortical, striatal and limbic forebrain circuitry. Neuroscience, 219, 120–36. 10.1016/j.neuroscience.2012.04.067 [PubMed: 22575585]

Vertes RP, Linley SB, & Hoover WB (2015). Limbic circuitry of the midline thalamus. Neurosci Biobehav Rev, 54, 89–107. 10.1016/j.neubiorev.2015.01.014 [PubMed: 25616182]

Woodson W, Farb CR, & LeDoux JE (2000). Afferents from the auditory thalamus synapse on inhibitory interneurons in the lateral nucleus of the amygdala. Synapse, 38(2), 124–37. 10.1002/1098-2396(200011)38:2<124::AID-SYN3>3.0.CO;2-N [PubMed: 11018786]

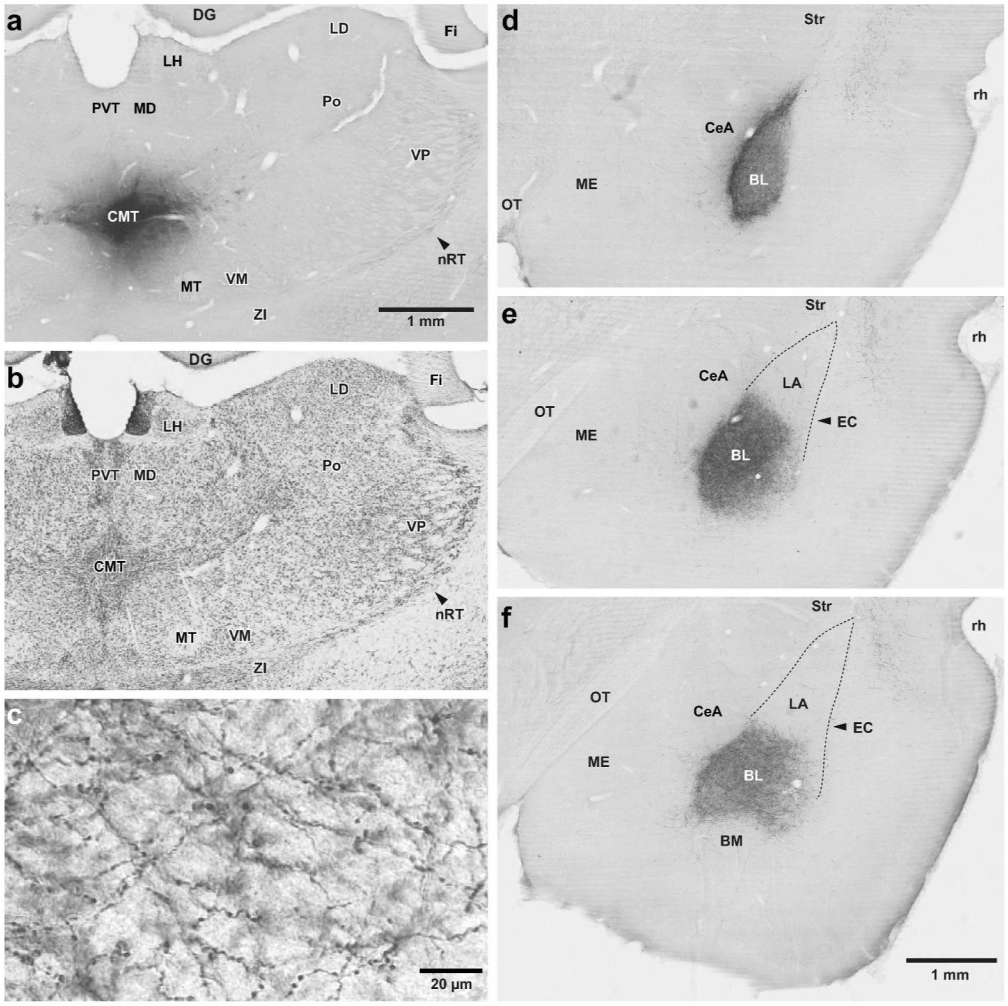

Figure 1.

CMT projections to the amygdala are largely confined to the basolateral nucleus (BL). (**a,b**) Two adjacent coronal sections processed to revealed the PHAL injection site in CMT (a) or the localization of thalamic nuclei in a Nissl-stained section (c) adjacent to that shown in a. (c) High power photomicrograph showing varicose PHAL-containing CMT axons ramifying in BL. (d-f) Three coronal sections showing the distribution of anterogradely labeled PHAL-immunoreactive CMT axons at rostral (d), intermediate (e), and caudal (f) levels of BL. Abbreviations: BL, basolateral nucleus of the amygdala; BM, basomedial nucleus of the amygdala; CeA, central nucleus of the amygdala CMT, central medial thalamic nucleus; DG, dentate gyrus; EC, external capsule; Fi, fimbria; LA, lateral nucleus of the amygdala; LD, laterodorsal thalamic nucleus; LH, Lateral habenula; MD, mediodorsal thalamic nucleus; ME, medial nucleus of the amygdala; MT, mammillothalamic tract; OT, Optic tract; nRT, reticular thalamic nucleus; Po, posterior thalamic nuclear group; PVT, paraventricular thalamic nucleus; rh, rhinal sulcus; Str, striatum; VM, ventromedial thalamic nucleus; VP, ventroposterior thalamic nucleus; ZI, zona incerta. Scale bar in a also applies to b. Scale bar in f also applies to d and e.

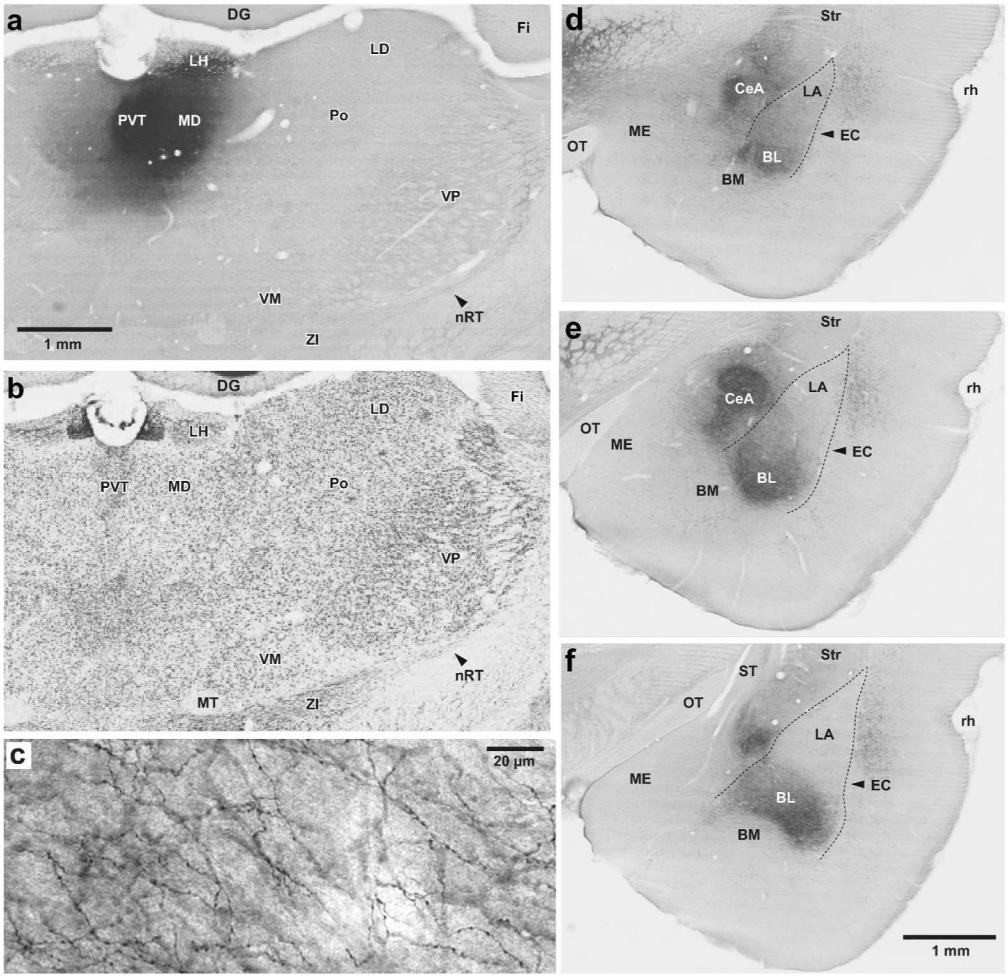

Figure 2.

PVT projections to the amygdala target both, the central (CeA) and basolateral (BL) nuclei. (a,b) Two adjacent coronal sections processed to revealed the PHAL injection site in PVT (a) or the localization of thalamic nuclei in a Nissl-stained section (b) adjacent to that shown in a. (c) High power photomicrograph showing varicose PVT axons ramifying in BL. (d-f) Three coronal sections showing the distribution of anterogradely labeled PVT axons at rostral (d), intermediate (e), and caudal (f) levels of the CeA and BL. Abbreviations: BL, basolateral nucleus of the amygdala; BM, basomedial nucleus of the amygdala; CeA, central nucleus of the amygdala CMT, central medial thalamic nucleus; DG, dentate gyrus; EC, external capsule; Fi, fimbria; LA, lateral nucleus of the amygdala; LD, laterodorsal thalamic nucleus; LH, Lateral habenula; MD, mediodorsal thalamic nucleus; ME, medial nucleus of the amygdala; MT, mammillothalamic tract; OT, Optic tract; nRT, reticular thalamic nucleus; Po, posterior thalamic nuclear group; PVT, paraventricular thalamic nucleus; rh, rhinal sulcus; Str, striatum; VM, ventromedial thalamic nucleus; VP, ventroposterior thalamic nucleus; ZI, zona incerta. Scale bar in a also applies to b. Scale bar in f also applies to d and e.

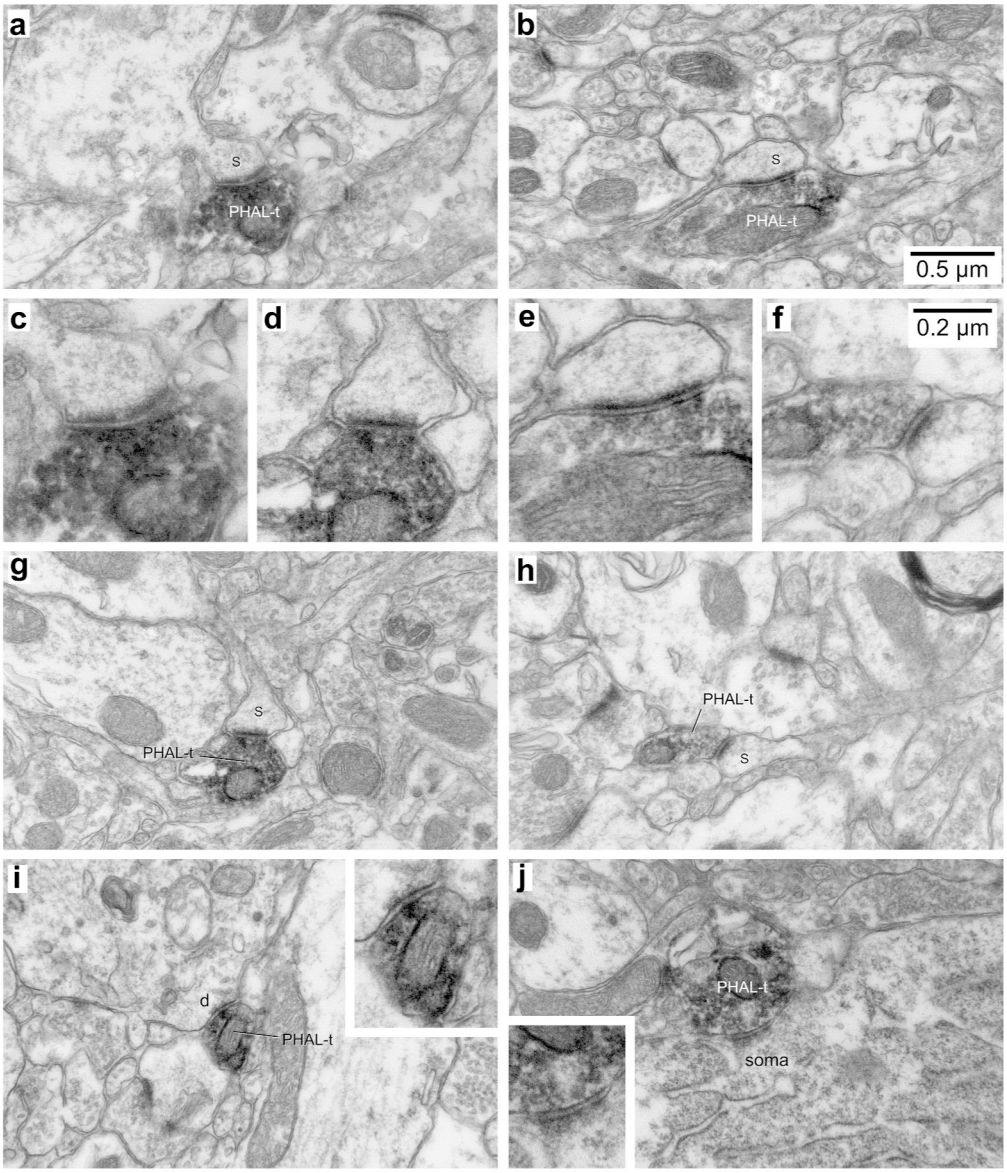

Figure 3.

Examples of synapses formed by PHAL-labeled CMT axon terminals in BL. (a,b,g,h) Four examples of PHAL-labeled axon terminals (PHAL-t) forming asymmetric synapses with dendritic spines (s). They are also shown at high magnification (c,d,e,f). In the cases shown in a and g, the spine targeted by the CMT axon terminal emerges from a large dendritic profile. In b, a long spine neck is evident. (i) Rare example of a CMT axon terminal forming an asymmetric synapse with a dendritic profile (d). Inset in i shows the same synapse at a higher magnification. (j) Sole example of a CMT axon terminal forming an asymmetric synapse with a somatic profile (soma). Inset in j shows the same synapse at a higher magnification. Scale bars in b and f apply to all low and high power electron micrographs, respectively.

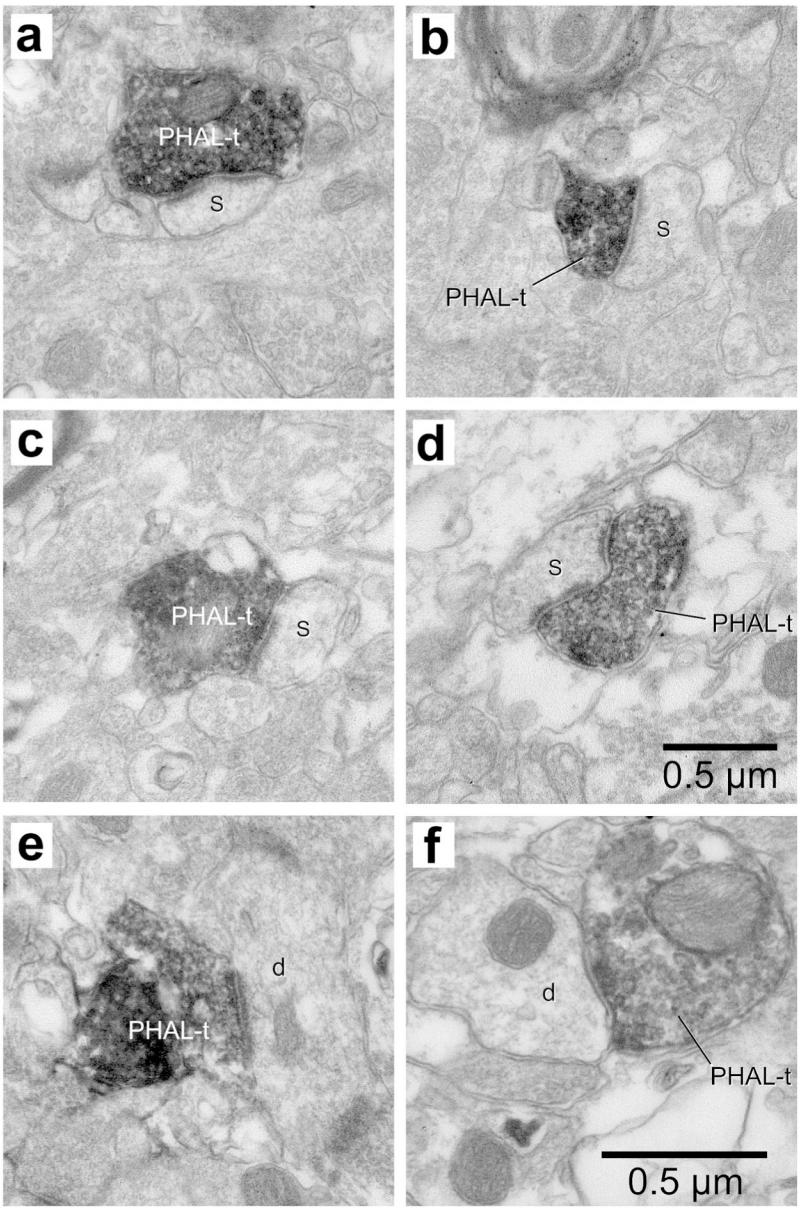

Figure 4.

Examples of synapses formed by PHAL-labeled PVT axons terminals in BL. (a-d) Four examples of PHAL-labeled axon terminals (PHAL-t) forming asymmetric synapses with dendritic spines (s). (e) Example of PVT axon terminal forming an asymmetric synapse with a dendritic profile (d). (f) The sole example of PVT axon terminal forming a symmetric synapse with a dendritic profile (d). Scale bar in d applies to panels a-d. Scale bar in f applies to panels e and f.

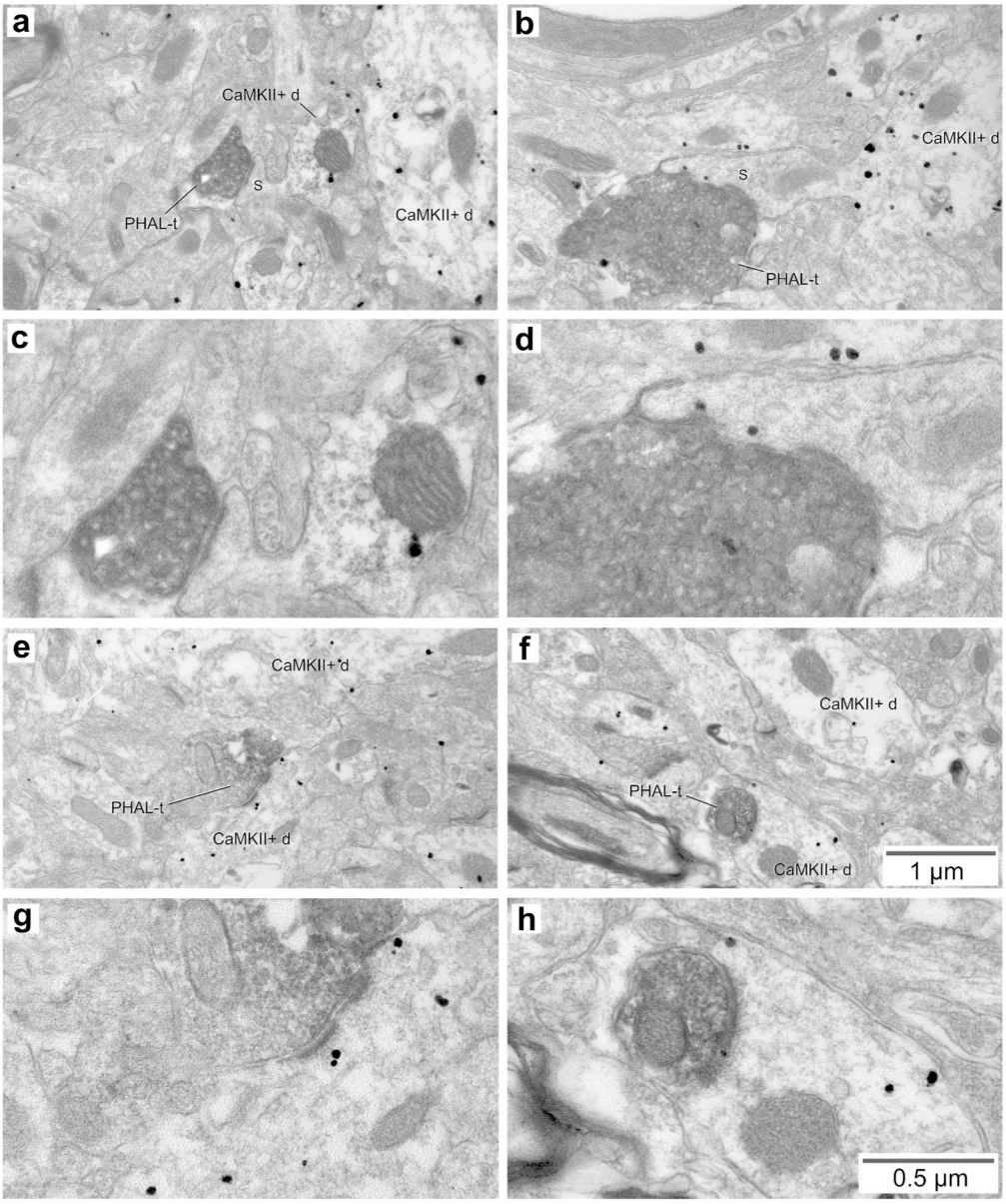

Figure 5.

Relationship between PHAL-labeled CMT axon terminals and CaMKIIa-immunopositive elements in BL. (a, b) Two examples of PHAL-positive CMT axon terminals (PHAL-t) forming asymmetric synapses with dendritic spines that emerge from CaMKIIa-immunopositive dendritic profiles (CaMKII+d). These synapses are also shown at high magnification (c,d). In a, the spine is devoid of gold particles, but it emerges from a labeled dendritic profile. In b, gold particles are present in both the spine and dendrite. (e, f) Two examples of PHAL-positive CMT axon terminals (PHAL-t) forming asymmetric synapses with CaMKIIa-immunopositive dendritic profiles. These synapses are also shown at high magnification (g,h). Scale bars in f and h apply to all low and high power electron micrographs, respectively.

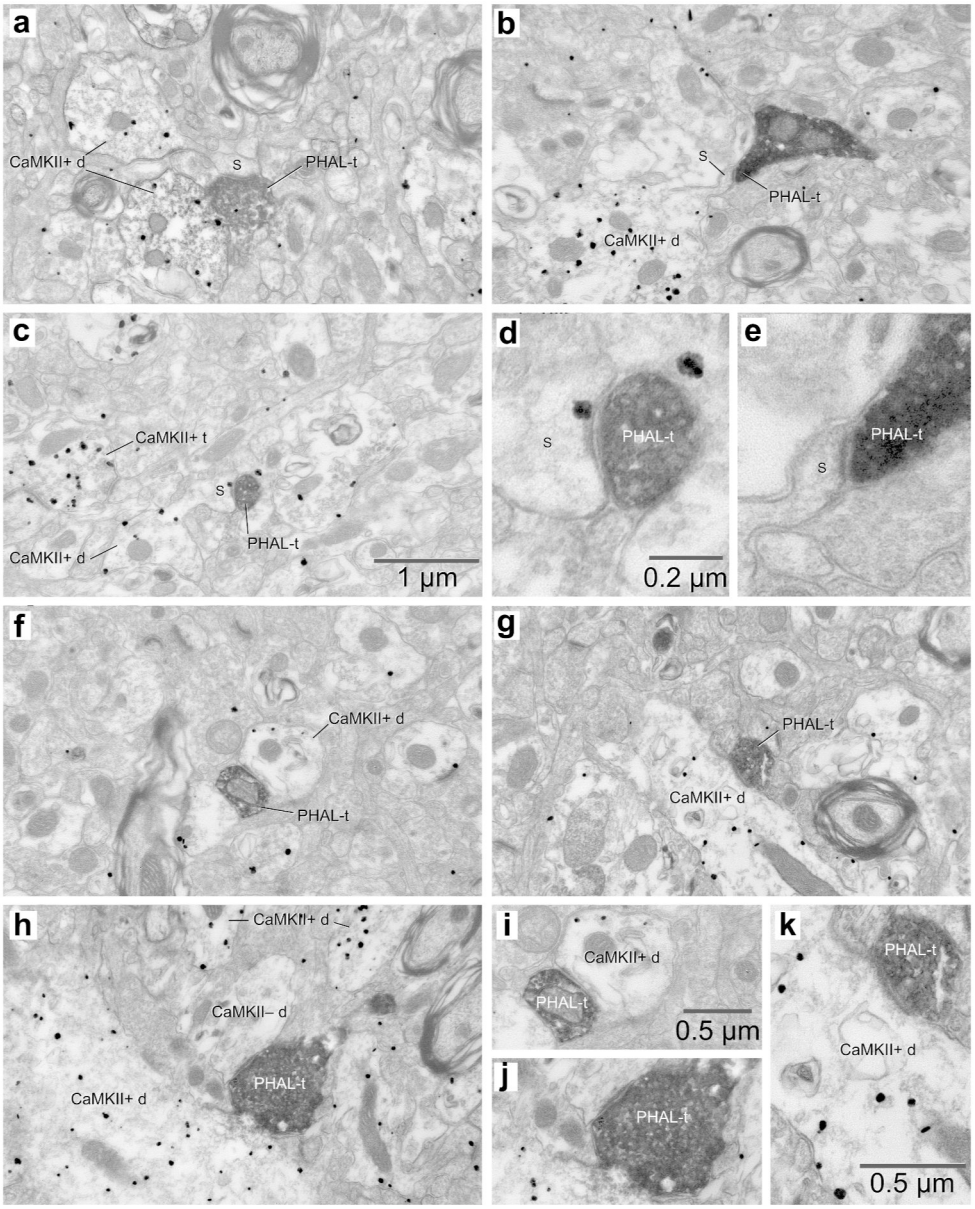

Figure 6.

Relationship between PHAL-labeled PVT axon terminals and CaMKIIa-immunopositive elements in BL. (a-c) Three examples of PHAL-positive PVT axon terminals (PHAL-t) forming asymmetric synapses with dendritic spines that emerge from CaMKIIa-immunopositive dendritic profiles (CaMKII+d). Synapses in b and c are also shown at high magnification (d,e). (f, g) Two examples of PHAL-positive PVT axon terminals (PHAL-t) forming asymmetric synapses with CaMKIIa-immunopositive dendritic profiles. These synapses are shown at a higher magnification (i,k). (h) Example of a PHAL-positive PVT axon terminal (PHAL-t) forming an asymmetric synapse with CaMKIIa-immunonegative dendritic profile (CaMKII– d). This synapse is shown at a higher magnification (j). Scale bar in c also applies to a, b f, g, h. Scale bar in d also applies to e. Scale bar in i also applies to j.

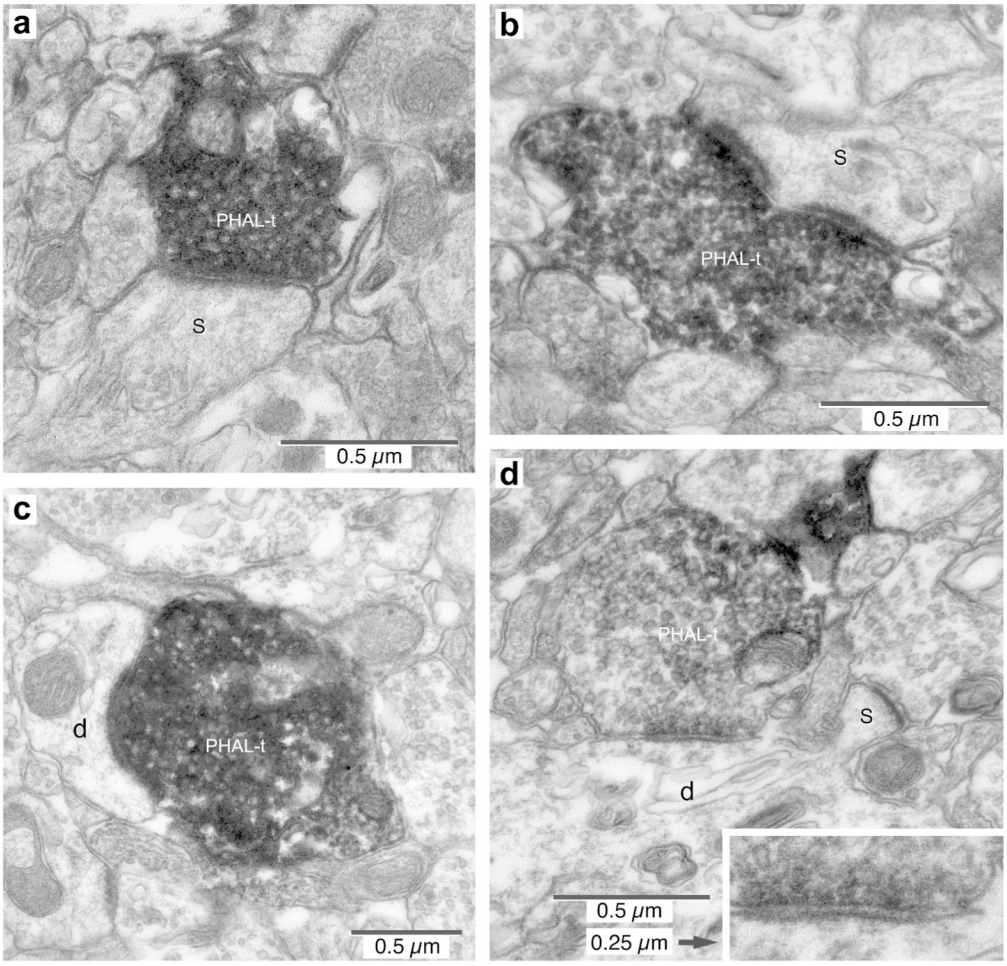

Figure 7.

Examples of synapses formed by PHAL-labeled PVT axons terminals in CeA. (a-b) Two examples of PHAL-labeled axon terminals (PHAL-t) forming asymmetric synapses with dendritic spines (s). (c) Example of PHAL-t forming an asymmetric synapse with a dendritic shaft (d). (d) Rare example of PHAL-t forming a symmetric synapse with a dendritic shaft (d). A spine (s) can be seen to emerge from this dendrite. Inset in d, magnified view of the same synapse.

TABLE 1

Number and proportion of different types of synapses (top row) formed by PHAL-positive CMT (second row) or PVT (third row) axon terminals in the BL nucleus.

	AC	AD	AS	SC	SD	SS	Total
CMT	1 (0.41%)	7 (2.9%)	233 (96.68%)	0 (0%)	0 (0%)	0 (0%)	241
PVT	0 (0%)	8 (8.6%)	84 (90.3%)	0 (0%)	1 (1.07%)	0 (0%)	93

Abbreviations: AC, asymmetric synapse on cell body; AD, asymmetric on dendrite; AS, asymmetric synapse on spine; SC, symmetric synapse on cell body; SD, symmetric synapse on dendrite; SS, symmetric synapse on spine.